Fitting Mid-Spatial Frequency Surface Errors with a Rapidly Decaying Fourier Series

Luke A. DeMars^{1,*}, Santiago Rueda¹, Miguel A. Alonso², and Thomas J. Suleski¹

¹Department of Physics and Optical Science, University of North Carolina at Charlotte, Charlotte, North Carolina 28223, USA
²Aix Marseille Univ., CNRS, Centrale Marseille, Institut Fresnel, UMR 7249, 13397 Marseille Cedex 20, France
*ldemars@uncc.edu

Abstract: We apply the $N_b=1$ solution of the Rapidly Decaying Fourier series to fit mid-spatial frequency surface errors. Using this basis enables definition of sharp spatial frequency bandlimits for mid-spatial frequency specification of optical surfaces. © 2023 The Author(s)

1. Introduction

Residual mid-spatial frequency (MSF) surface errors are consequences of sub-aperture manufacturing methods used for the fabrication of radially symmetric and freeform optics [1]. Orthogonal decomposition of MSF errors has previously been investigated to better understand and specify MSF errors on optical surfaces with a range of basis sets for circular apertures [2,3], square apertures [4], and arbitrary apertures [5–8].

In this work, we consider the $N_b = 1$ solution of the Rapidly Decaying Fourier (RDF) series for circular apertures[9]. A benefit of this basis is its ability to produce sharp cutoffs in the frequency domain that enable definition of spatial frequency bandlimits with little residual error beyond that specified bandlimit. To illustrate this point, we first show relationships between the period and distribution of the MSF surface error and the amplitude coefficients of the $N_b = 1$ RDF basis using a map visualization method used in previous work [2–4]. We then compare the polar areal power spectral density (PSD) and the residual polar areal PSD [10,11] of a fitted experimental MSF surface to demonstrate the sharp cutoffs in the frequency domain.

2. Methods

The RDF $N_b=1$ basis is defined by Eq. 1, where c_n^m is the amplitude coefficient, and the radial and azimuthal components are defined in Eqs. 2 and 3, respectively. The n=0 piston term in Eq. 1 is not included because it does not capture surface oscillations. In Eq. 2, R is the surface radius, and the α_n^m term in Eq. 2 describes the zeros crossing and is approximately equal to the spatial frequency of the surface error.

$$\mu(r,\phi) = \sum_{m=-M_{\text{max}}/2}^{M_{\text{max}}/2} \sum_{n=1}^{n=N_{\text{max}}} c_n^m \mathfrak{R}_n^m(r) \Phi_m(\phi)$$
 (1)

$$\mathfrak{R}_n^m(r) = \frac{\sqrt{2}J_m(\alpha_n^m r)}{R\sqrt{J_m^2(\alpha_n^m r) - J_{m-1}^2(\alpha_n^m r)}}$$
(2)

$$\Phi_{m}(\phi) = 1 / \sqrt{\pi} \begin{cases}
1 / \sqrt{2} & m = 0 \\
\cos(m\phi) & m > 0 \\
\sin(|m|\phi) & m < 0
\end{cases}$$
(3)

A least squares procedure in MATLAB is used to fit this basis to an MSF surface error, and the c_n^m coefficients are plotted in a "coefficient map" where the x and y axis displays the n and m order for a particular coefficient, and the coefficient amplitudes are encoded in the z-axis. In Fig. 1, we show three purely sinusoidal MSF signatures distributions (radial, azimuthal, and raster), each with 200 nm amplitude. We highlight the peak locations in Fig.1 to illustrate the relationship between the coefficient peaks and the period and distribution of the MSF surface errors. Note that (1) the radial MSF error peaks in n value at m = 0 when n is equal to the number of radial oscillations across the part; (2) the azimuthal MSF error peaks in m at n = 1 when m equals the number of oscillations around the perimeter of the surface; (3) the linear raster MSF errors peaks follow a curved line starting at the intercept of n equal to the number of raster oscillations and ending approximately at the intercept of m equal to π times the number of raster oscillations.

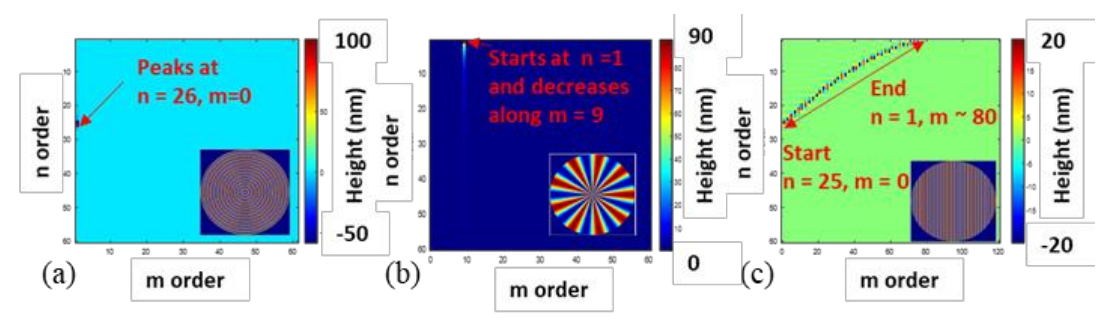


Fig. 1. (a) Coefficient map of C_n^m values for radial MSF with 26 cycles across the part; (b) Coefficient map of C_n^m values for azimuthal MSF with 9 cycles around the perimeter of the part; (c) Coefficient map of C_n^m values for raster MSF with 25 cycles across the part. Note: the three color bar ranges are not equal.

3. Results and Discussion

In this example, we demonstrate fitting an experimental MSF surface error shown in Fig. 2(a) from 0.11 cyc/mm to 10 cyc/mm. To capture both the radial and linear raster MSF errors in the surface, we fit from $1 \le n \le 90$, and $-284 \le m \le 284$ along a slope magnitude of π from the n and m intercepts, as shown in Fig. 2(b). Fig. 2(c) shows the reconstructed surface and its polar areal PSD. In Fig. 2(d), we show the residual surface and its polar Areal PSD.

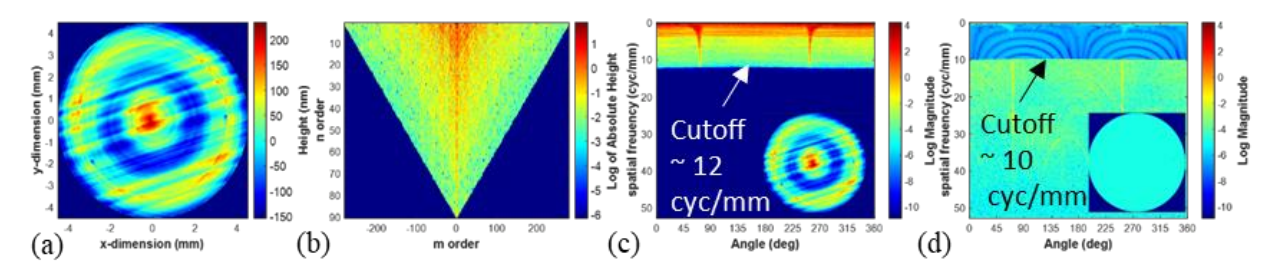


Fig. 2. (a) Complex MSF with both raster and radial errors with a diameter of 9 mm; (b) coefficient map fitted MSF surface error (c) fitted surface (scaled to Fig. 2(a)) and polar areal PSD of the fitted surface; (d) residual surface (scaled to Fig. 2(a)) and polar areal PSD of the residual surface.

We note the difference in the cutoff spatial frequencies in the fitted spectra (12 cyc/mm) and the residual spectra (10 cyc/mm) due to the linear approximation for the slope magnitude. Additional work is needed to determine a non-linear relationship between n and m to better match cutoff frequencies, resulting in a tighter band-limit specification.

4. Acknowledgements

The authors would like to acknowledge useful discussions with Dr. Greg Forbes from Macquarie University and Dr. Aaron Bauer and Dr. Jannick Rolland from the University of Rochester. This work was funded by the NSF I/UCRC Center for Freeform Optics (IIP-1822049, and IIP-1822026).

5. References

- [1] J. P. Rolland, M. A. Davies, T. J. Suleski, C. Evans, A. Bauer, J. C. Lambropoulos, and K. Falaggis, "Freeform optics for imaging," Optica 8, 161 (2021).
- [2] G. W. Forbes, "Never-ending struggles with mid-spatial frequencies," Proc. SPIE 9525, 95251B (2015).
- [3] Z. Hosseinimakarem, A. D. Davies, and C. J. Evans, "Zernike polynomials for mid-spatial frequency representation on optical surfaces," Proc. SPIE 9961, 99610P (2016)
- [4] W. Fei, L. Zhao, J. Bai, X. Zhou, J. Hou, H. Yan, and K. Wang, "Feature-based characterization and extraction of ripple errors over the large square aperture," Opt. Express 29, 8296 (2021).
- [5] M. Maksimovic, "Optical tolerancing of structured mid-spatial frequency errors on free-form surfaces using anisotropic radial basis functions," Proc. SPIE 9626, 962613 (2015).
- [6] J. Stock, A. Broemel, J. Hartung, D. Ochse, and H. Gross, "Description and reimplementation of real freeform surfaces," Appl Opt **56**, 391 (2017).
- [7] G. M. Marshall, "Orthogonal mode decomposition of aspheric surface form errors by principal components analysis," Opt. Eng. 57, 124103
- [8] X. Zhou, X. Huang, J. Bai, L. Zhao, J. Hou, K. Wang, and Y. Hua, "Representation of complex optical surfaces with adaptive radial basis functions," Appl. Opt. 58, 3938 (2019).
- [9] K. Liang, G. W. Forbes, and M. A. Alonso, "Rapidly decaying Fourier-like bases," Opt Express 27, 32263 (2019).
- [10] T. Pertermann, J. Hartung, M. Beier, M. Trost, S. Schröder, S. Risse, R. Eberhardt, A. Tünnermann, and H. Gross, "Angular resolved power spectral density analysis for improving mirror manufacturing," Appl. Opt. 57, 8692 (2018).
- [11] L. A. DeMars and T. J. Suleski, "Separating and Estimating Impacts of Anisotrpic mid-spatial frequency errors," in OSA Optical Design and Fabrication 2021 (Flat Optics, Freeform, IODC, OFT), (Optica Publishing Group, 2021), paper OW3B.2.